Impact of antiferromagnetic order on Landau-level splitting of quasi-two-dimensional Dirac fermions in EuMnBi_{2}

H. Masuda, H. Sakai, M. Tokunaga, M. Ochi, H. Takahashi, K. Akiba, A. Miyake, K. Kuroki, Y. Tokura, and S. Ishiwata

Phys. Rev. B **98**, 161108 — Published 9 October 2018

DOI: 10.1103/PhysRevB.98.161108

Impact of antiferromagnetic order on Landau level splitting of quasi-two-dimensional Dirac fermions in $EuMnBi_2$

H. Masuda[1], H. Sakai[2,3],* M. Tokunaga[4], M. Ochi[2], H. Takahashi[1],
K. Akiba[4], A. Miyake[4], K. Kuroki[2], Y. Tokura[1,5], and S. Ishiwata[1,3]

[1]*Department of Applied Physics, University of Tokyo, Tokyo 113-8656, Japan.*

[2]*Department of Physics, Osaka University,*
Toyonaka, Osaka 560-0043, Japan.

[3]*PRESTO, Japan Science and Technology Agency,*
Kawaguchi, Saitama 332-0012, Japan.

[4]*The Institute for Solid State Physics,*
University of Tokyo, Kashiwa 277-8581, Japan.

[5]*RIKEN Center for Emergent Matter Science (CEMS), Wako 351-0198, Japan.*

Abstract

We report spin-split Landau levels of quasi-two-dimensional Dirac fermions in a layered antiferromagnet $EuMnBi_2$, as revealed by interlayer resistivity measurements in a tilted magnetic field up to $\sim$35 T. The amplitude of Shubnikov-de Haas (SdH) oscillation in interlayer resistivity is strongly modulated by changing the tilt angle of the field, i.e., the Zeeman-to-cyclotron energy ratio. The effective g factor estimated from the tilt angle, where the SdH oscillation exhibits a phase inversion, differs by approximately 50% between two antiferromagnetic phases. This observation signifies a marked impact of the magnetic order of Eu sublattice on the Dirac-like band structure. The origin may be sought in strong exchange coupling with the local Eu moments, as verified by the first-principles calculation.

Dirac fermions in solids have attracted extensive attention for their unusual quantum transport phenomena[1], typified by a half-integer quantum Hall effect in graphene[2, 3]. As a bulk analogue of graphene, so-called Dirac and Weyl semimetals hosting linear energy dispersion are recently of particular interest[4]. One of the greatest advantages of their bulk form is the interplay of relativistic quasiparticles with magnetism, which potentially leads to novel (spin)electronic applications[5, 6]. Recently, a few candidates of Dirac or Weyl magnets were reported, as exemplified by Mn_3Sn[7, 8], GdPtBi[9, 10], and pyrochlore iridates[11, 12]. Some of these materials were found to exhibit peculiar magneto-transport phenomena, such as large anomalous Hall effects[7–9] and chiral anomalies[10, 13], consistent with the theoretically-predicted Weyl semimetal states. For exploring their potential applications, the roles of magnetic order on the topological electronic and transport properties need to be experimentally elucidated, which remains a work in progress[13].

AMnX_2 (A: alkaline-earth and rare-earth ions, X: Bi and Sb)[14–26] is also promising as a fertile ground for magnetic Dirac materials, since the crystal structure consists of an alternate stack of a two-dimensional (2D) Dirac fermion conduction layer (X^- square net)[27, 28] and a magnetic insulating layer (A^{2+}-Mn^{2+}-X^{3-}) [see Fig. 1(a)]. Among them, $EuMnBi_2$ is a rare compound that exhibits quantum transport of Dirac fermions coupled with the field-tunable magnetic order. In this compound, the interlayer coupling between each Dirac fermion (Bi) layer is dramatically suppressed by the flop of the antiferromagnetically-ordered Eu moments [Fig. 1(a)]. The enhanced two dimensionality leads to the giant magnetoresistance effects[20, 21] and the quantum oscillation phenomena[21] that strongly depend on the magnetic order of the Eu sublattice. However, in spite of such a marked impact of magnetism on the transport properties, it remains elusive how and to what extent the Dirac-like band dispersion is affected.

To reveal the coupling between the band structure and magnetic order, the Landau level quantization in a magnetic field can be a powerful probe, since it exhibits the energy splitting due to Zeeman and exchange coupling as well as electron-electron interaction. As demonstrated in the conventional 2D electron gas in semiconductor heterostructures[29] and semimagnetic quantum wells[30], the detailed analyses on the splitting provide lots of information on the band parameters and magnetism of the system, which have been recently performed for graphene[31, 32] and several Dirac semimetals[33–35]. Also for $EuMnBi_2$, clear Landau level splitting was observed in the SdH oscillation in resistivity[21], the origin

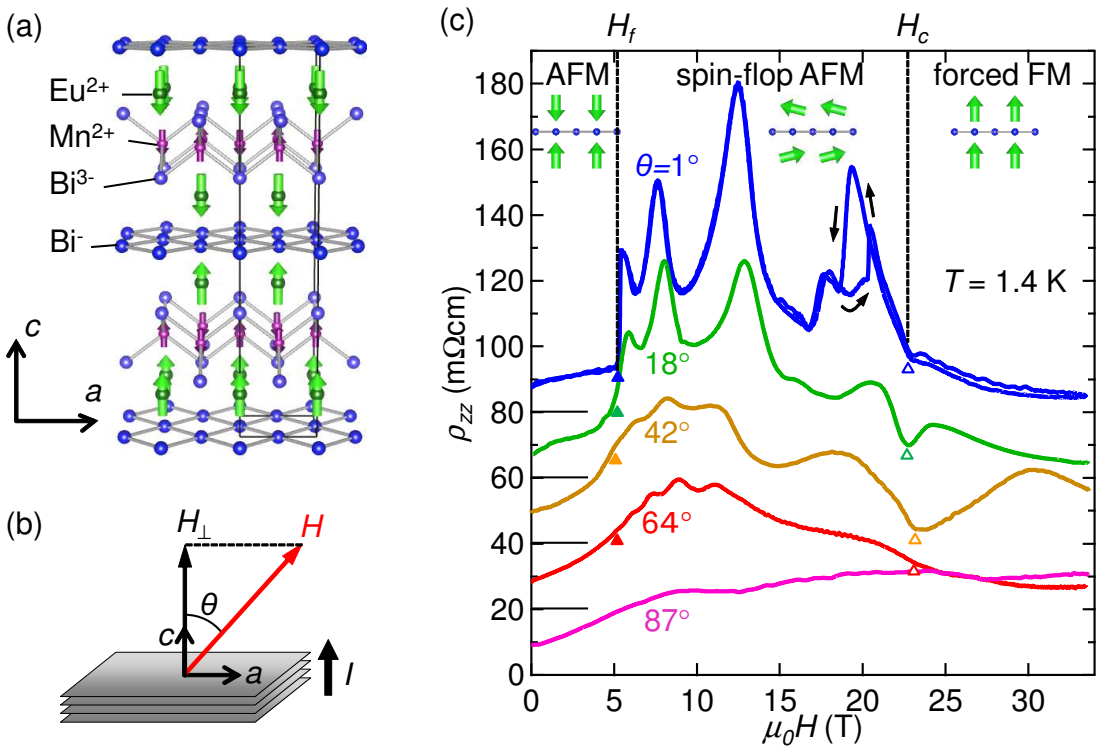

FIG. 1: (Color online) (a) Schematic illustration of the crystal and magnetic structure at 0 T for $EuMnBi_2$ [21, 36]. (b) Geometry of the interlayer transport measurement in a tilted magnetic field in the a-c plane, where θ is an angle between the field and the c axis. (c) Field profile of ρ_{zz} at 1.4 K for selected values of θ. For clarity, the curves are shifted vertically by 20 mΩcm. For $\theta < 64°$, the closed triangle denotes $H_{\rm f}$ while the open triangle denotes $H_{\rm c}$. The positions of $H_{\rm f}$ and $H_{\rm c}$ are determined as the fields where ρ_{zz} shows a jump and drop in the field-increasing run, respectively. For details, see supplementary Fig. S1. The magnetic order of the Eu sublattice for each antiferromagnetic phase is shown schematically in the inset.

of which has not been clarified so far. In this Letter, we clarify that the Landau level splitting in $EuMnBi_2$ is primarily of spin origin, on the basis of the systematic measurements of the SdH oscillations in tilted magnetic fields. The field-angle dependence of SdH oscillations have revealed the effective g factors for the Dirac fermions, which strongly depends on the antiferromagnetic (AFM) order of the Eu sublattice. As a plausible explanation, we discuss the exchange coupling between Dirac fermions and local Eu moments by considering the results of the first-principles calculations.

For investigating the fine structures of Landau levels, we have here adopted the measure-

ments of interlayer resistivity ρ_{zz}. This is because the high-resistive ρ_{zz} has a much better S/N ratio than that achieved in the in-plane resistivity ρ_{xx}. A rotation of magnetic field is also important in the present study. In 2D systems, the ratio of the cyclotron energy $E_{\rm c}$ to the Zeeman energy $E_{\rm Z}$ can be tuned by changing the tilt angle of the field from the normal to the 2D plane (θ); $E_{\rm c}$ is proportional to $H_\perp = H\cos\theta$ [the field component perpendicular to the 2D plane, see Fig. 1(b)], while $E_{\rm Z}$ is proportional to H (the total field). The combination of these techniques allow us to elucidate the mechanism of the Landau level splitting and hence the microscopic nature of the Dirac fermions in $EuMnBi_2$, as described below.

Figure 1(c) shows the field dependence of interlayer resistivity ρ_{zz} for $EuMnBi_2$ up to 35 T at selected tilt angles of the field. We first review the transport features for the field parallel to the c axis (at $\theta = 1^\circ$). With increasing the field, ρ_{zz} exhibits a steep jump at the spin-flop transition of the Eu sublattice ($H_f \sim 5.3$ T), followed by large SdH oscillations. In the forced ferromagnetic (FM) phase above $H_{\rm c}\sim$22 T, however, the value of ρ_{zz} significantly decreases, indicating that ρ_{zz} is specifically enhanced in the spin-flop AFM phase. There, the Dirac fermions in the Bi layer are strongly confined in two dimension, resulting in the signature of multilayer half-integer quantum Hall effect in the in-plane conductions[21].

Similar enhancement in ρ_{zz} in the spin-flop AFM phase was observed at θ up to $\sim$65°, which is gradually reduced with increasing θ. Concomitantly, the spin-flop transition at $H_{\rm f}$ is less sharp at high θ, which is still discernible up to θ=64° as denoted by closed triangles in Fig. 1(c) (for the determination of $H_{\rm f}$, see supplementary Fig. S1). The manner of the SdH oscillation is also strongly dependent on θ, whereas the values of $H_{\rm f}$ and $H_{\rm c}$ are almost independent of θ. Note here that, in addition to the SdH oscillation, a hysteretic resistivity anomaly is discernible around 20 T at θ=1°, which immediately disappears when θ increases up to 18°. At present, the origin of this highly-θ-sensitive anomaly remains unclear, the study of which is beyond the scope of this paper. In the following, we shall focus on the θ dependence of the SdH oscillations in ρ_{zz}.

We first show in Fig. 2(a) the features of the Landau levels in the spin-flop AFM phase ($H_f < H < H_c$) by presenting the θ dependence of interlayer conductivity $\sigma_{zz} = 1/\rho_{zz}$[37]. The horizontal axis of Fig. 2(a) denotes $H_F^0/H_\perp$, the normalized filling factor for a 2D system[21, 42], where H_F^0(=19.3 T) is the SdH frequency for the field parallel to the c axis (Fig. S3)[38]. At θ=1°, σ_{zz} shows the minima at $H_F^0/H_\perp \simeq 1.5, 2.5, 3.5$, which coincides with the oscillations in σ_{xx} and ρ_{xx}[21]. Since the deep minima in σ_{zz} and σ_{xx} indicate the

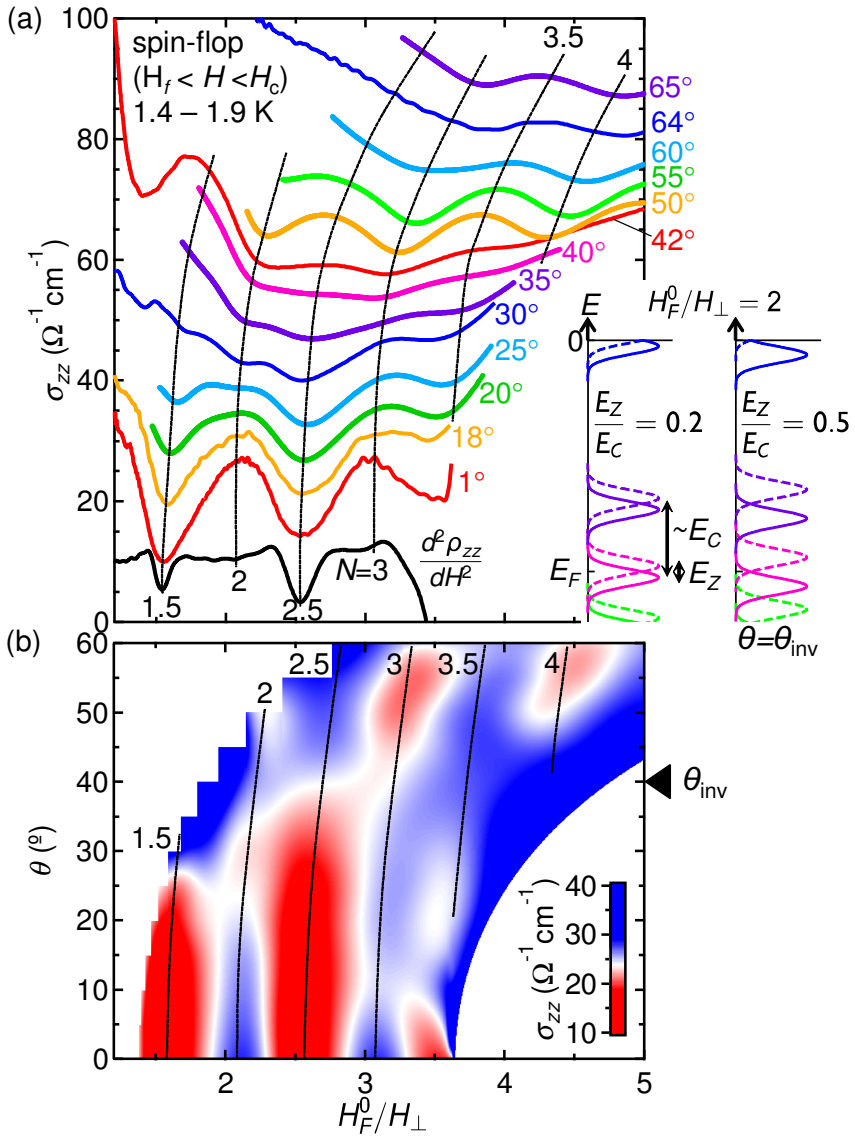

FIG. 2: (Color online) (a) σ_{zz} versus $H_F^0/H_\perp$ at θ=1°-65° in the spin-flop AFM phase ($H_f < H < H_c$), where H_F^0 denotes the SdH frequency for the field parallel to the c axis. The curves at $\theta \geq 18°$ are shifted upward for clarity. At the bottom of the panel, the second field derivative $d^2\rho_{zz}/dH^2$ at $\theta = 1°$ is shown. Vertical dotted lines are guides to the eye showing the positions of the maxima and minima of the SdH oscillation, where N denotes the Landau index. Inset: Schematic of the density of states for spin-split Landau levels for a 2D massless Dirac fermion as a function of energy E for $H_F^0/H_\perp = 2$, where $E_{\rm F}$ is set negative corresponding to the hole carrier system. The value of $E_{\rm Z}/E_{\rm c}$ can be tuned by tilting the field, where $E_{\rm Z} = g^*\mu_{\rm B}B$ is the Zeeman energy, $E_{\rm c} \equiv e\hbar B_\perp/m_{\rm c}$ the effective cyclotron energy, and $m_{\rm c}$ the cyclotron mass $m_{\rm c} = E_{\rm F}/v_{\rm F}^2$. $E_{\rm Z}/E_{\rm c} = 0.2$ (left) and 0.5 (right). For details of the calculation, see the main text and supplementary Fig. S4. (b) Color plot of σ_{zz} as functions of $H_F^0/H_\perp$ and θ. $\theta_{\rm inv}$ indicated by the triangle corresponds to θ where the phase of the SdH oscillation is inverted and $E_{\rm Z}/E_{\rm c}$ is nearly 0.5.

quantum Hall states[39–41], the corresponding $H_F^0/H_\perp$ should be given by $H_F^0/H_\perp = N + 1/2 - \gamma$, where N is the Landau index and γ is the phase factor expressed as $\gamma = 1/2 - \phi_B/2\pi$ with ϕ_B the Berry's phase[43]. The σ_{zz} minima occurring at half-integer multiples of $H_F^0/H_\perp$ thus lead to $\gamma \sim 0$, i.e., the nontrivial π Berry's phase in $EuMnBi_2$. In multilayer quantum Hall systems, it was reported that a chiral surface state contributes partly to the interlayer transport in the quantum Hall states (i.e., σ_{zz} minima)[39–41], which does not affect the frequency or phase of the SdH oscillation discussed below. When θ increases, the frequency of the SdH oscillation increases in proportion to $1/\cos\theta$ [Fig. S3(c)][38], indicating highly 2D nature of the Fermi surface. This results in the almost θ-independent oscillation period when plotted as a function of $H_F^0/H_\perp$, as highlighted by the vertical dotted lines up to $\theta \sim 50°$ in Fig. 2(a). For $\theta \geq 55°$, however, the frequency gradually deviates from the $1/\cos\theta$ scaling presumably due to a weak warping of the Fermi surface caused by the non-zero interlayer coupling.

The most salient feature of the SdH oscillation is that the amplitude significantly varies with θ. With increasing θ up to 35°-40°, the amplitude progressively decreases to nearly zero. Above $\theta = 40°$, the amplitude again increases but with an inverted phase. The observed θ dependence of the SdH amplitude is well explained by considering the spin splitting of the Landau levels due to E_Z as follows[44–46]. When E_Z/E_c is smaller than unity [e.g., $E_Z/E_c = 0.2$ in the inset (left) to Fig. 2(a)], the Landau level exhibits a weak spin splitting, which is barely discernible at $\theta \sim 1°$ when plotted in the form of $d^2\rho_{zz}/dH^2$ [Fig. 2(a)][21] . With increasing E_Z/E_c by tilting the field, the magnitude of the spin splitting increases, resulting in the reduction in amplitude of the SdH oscillation. Around $\theta = 40°$, the amplitude reaches the minimum, which corresponds to $E_Z/E_c = 0.5$ [the inset (right) to Fig. 2(a)]. A further increase in E_Z/E_c leads to crossing of the neighboring Landau levels with opposite spins, which results in the enhanced SdH oscillation with an inverted phase, as observed at $\theta > 50°$. Note here, since the energy spacing of Landau levels for a 2D Dirac fermion is not uniform (i.e., E_c is dependent on N), we need to effectively define $E_c \equiv e\hbar B_\perp/m_c$ by using a semiclassical expression of the cyclotron mass $m_c = E_F/v_F^2$ with v_F and E_F being the Fermi velocity and Fermi energy, respectively[2, 3]. In this scheme, the Landau level crossing in the SdH oscillation occurs when $E_Z/E_c = 1$ irrespective of N, as in the case for a normal 2D electron gas [for details, see Fig. S4(b)][38].

To highlight the θ dependence of the SdH oscillations, we present a contour plot of

σ_{zz} as functions of $H_F^0/H_\perp$ and θ in Fig. 2(b). It is clear that the phase of the SdH oscillation is inverted around $\theta_{\rm inv} \sim 40°$, accompanied by the minimum amplitude. As shown in supplementary Fig. S4(c)[38], this plot is nicely reproduced by calculating the density of states of spin-split Landau levels, where $E_{\rm Z}/E_{\rm c} = 0.5$ corresponds to $\theta = \theta_{\rm inv}$[47]. Noting that $E_{\rm Z}/E_{\rm c} = g^* m_{\rm c}/2m_0 \cos\theta$, this relation gives $\cos\theta_{\rm inv} = g^* m_{\rm c}/m_0$, where g^* is the effective g factor and m_0 is the bare electron mass. By substituting the experimental value ($\theta_{\rm inv} = 40° \pm 5°$), we obtain $g^* m_{\rm c}/m_0 = 0.77(6)$. The value of $m_{\rm c}/m_0$ is independently estimated to be 0.122(2) from the temperature dependence of the SdH oscillations at $\theta = 0°$ based on the standard Lifshitz-Kosevich formula (Fig. S8)[38], which results in $g^* = 6.6(6)$. The obtained g^* is much larger than 2, reflecting strong spin-orbit coupling inherent to Bi atom. Additionally, it is presumable that the exchange interaction with the local Eu moments plays a significant role, since net magnetization is non-zero in the spin-flop AFM phase, as discussed later.

Next, we shall show the Landau level splitting in the AFM phase ($H < H_f$), where the amplitude of SdH oscillation is largely reduced as compared with the spin-flop AFM phase. Nonetheless, the oscillation is discernible above ∼1.3 T, as shown in Fig. 3(b) where $d^2\rho_{zz}/dH^2$ is plotted for clarity. The weakly beating amplitude presumably signifies the superposition of maximum and minimum cyclotron orbits arising from a slightly warped cylindrical Fermi surface. To summarize the θ dependence of SdH oscillation, we show in Fig.3(a) the color contour plots of $d^2\rho_{zz}/dH^2$ and σ_{zz} for the AFM and spin-flop AFM phases, respectively, as functions of $H_F^0/H_\perp$ and θ. The SdH oscillation in the AFM phase has several common features with that in the spin-flop AFM phase; the period of the SdH oscillation is nearly independent of θ when plotted versus $1/H_\perp$, reflecting a quasi-2D Fermi surface. In addition, the spin splitting of the Landau levels makes the oscillation amplitude dependent on θ, leading to the phase inversion at $\theta_{\rm inv}$ (a horizontal line). However, the value of $\theta_{\rm inv}$ is substantially different in the two phases; $\theta_{\rm inv} \sim 18°$ for the AFM phase while $\theta_{\rm inv} \sim 40°$ for the spin-flop AFM phase. This results in $g^* m_c/m_0 = \cos\theta_{\rm inv} = 0.95(1)$ for the AFM phase ($\theta_{\rm inv} = 18° \pm 2°$), which is approximately 25% larger than that for the spin-flop AFM phase.

In Table I, we compare the band parameters estimated from the SdH oscillation for each AFM phase. The cross section of quasi-2D Fermi surface $S_{\rm F}$ deduced from the SdH frequency (H_F^0) is almost the same for both AFM phases, whereas the values of $m_{\rm c}$ and g^* significantly

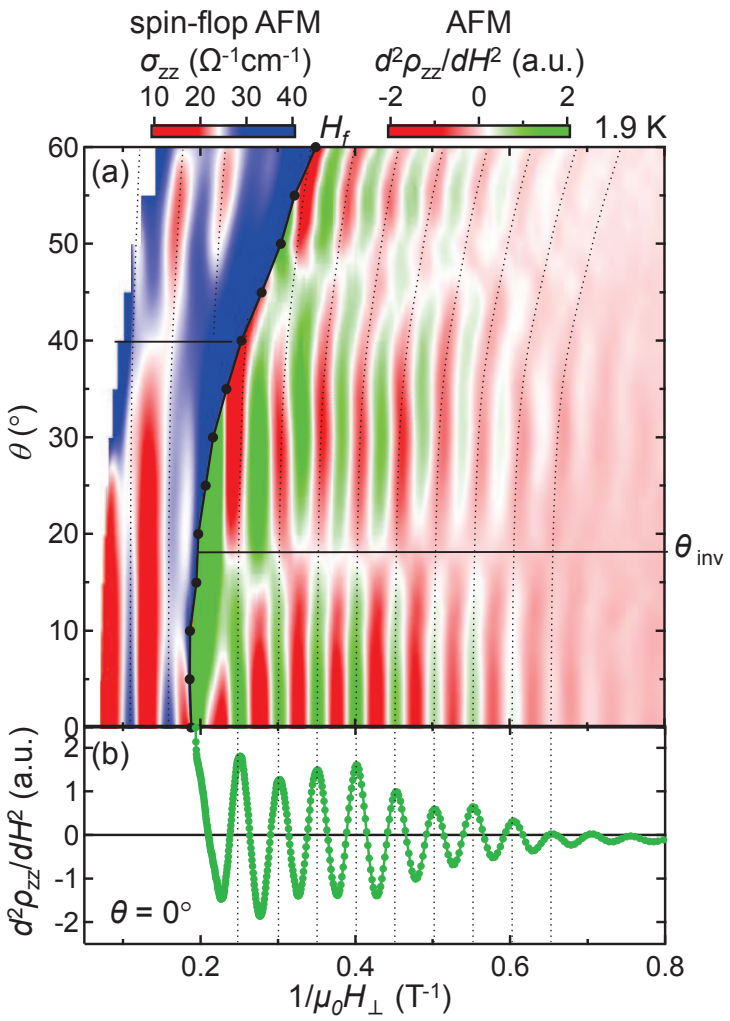

FIG. 3: (Color online) (a) Color plot of $d^2\rho_{zz}/dH^2$ as functions of $H_F^0/H_\perp$ and θ in the AFM phase (for $H < H_f$). To compare the θ dependence, the σ_{zz} data in the spin-flop AFM phase (for $H > H_f$) are plotted together. The position of $H_{\rm f}$ at each θ is denoted by a closed circle, which is determined as the field where ρ_{zz} shows a steep increase (see supplementary Fig. S1). The horizontal line denotes $\theta_{\rm inv}$ for each phase. (b) Profile of $d^2\rho_{zz}/dH^2$ versus $H_F^0/H_\perp$ for $\theta = 0°$ ($H < H_f$).

depend on the AFM order. Since the AFM phase hosts larger $g^* m_{\rm c}/m_0$ and smaller $m_{\rm c}/m_0$ than the spin-flop AFM phase, the resultant g^* value for the former phase is approximately 50% larger than that for the latter phase. These facts indicate that the Dirac-like band for $EuMnBi_2$ is largely modulated by the AFM order of Eu sublattice.

First-principles calculations indeed reproduce such a marked dependence of the band

TABLE I: Experimentally determined band parameters for the AFM and spin-flop AFM phases. For the estimation of S_F and m_c, see supplementary Figs. S3 and S6−S10.

	S_F (nm^{-2})	$g^* m_c/m_0$	m_c/m_0	g^*
AFM	0.186	0.95(1)	0.097(2)	9.8(4)
spin-flop	0.191	0.77(1)	0.122(2)	6.6(4)

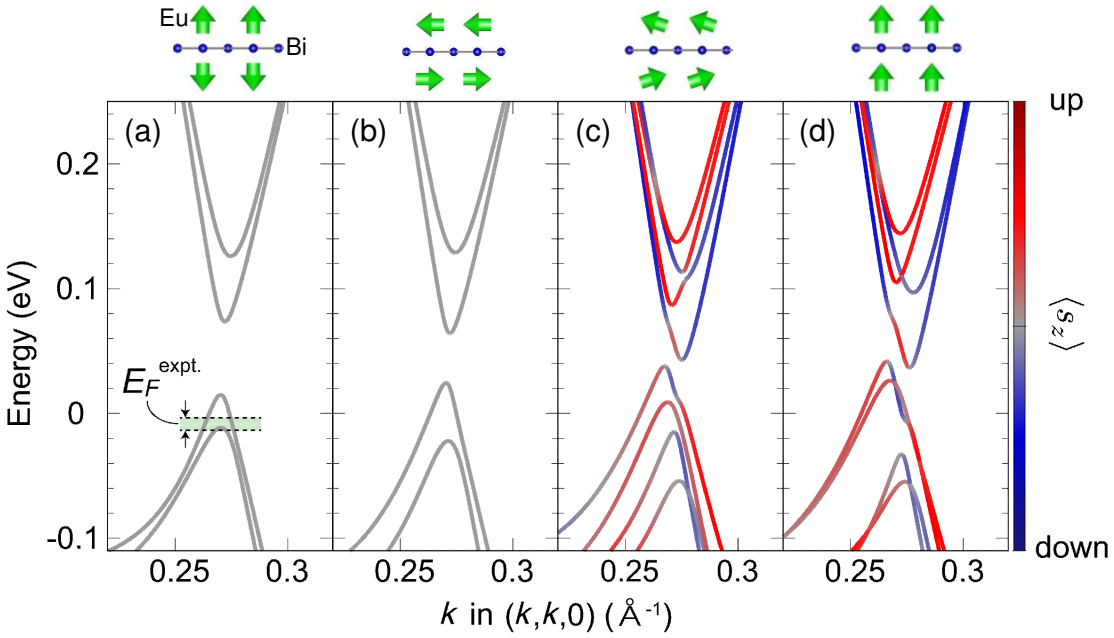

FIG. 4: (Color online) Calculated Dirac-like band structures along the Γ-M line for various magnetic states in $EuMnBi_2$. (a) AFM, (b, c) spin-flop AFM, and (d) forced FM states. In (b), the Eu moment is along the a axis, while in (c) it is inclined at an angle of ∼47° to the c axis on the ac plane. The spin polarization $\langle s_z \rangle$ of each band is represented by red (up) and blue (down) colors. Schematic illustration of the Eu moments adjacent to the Bi layer is also shown. The Fermi energy E_F estimated from the experimental SdH oscillation is denoted by the shaded area in (a). For details, see supplementary Fig. S12

structure on the magnetic state, as shown in Fig. 4, where the Dirac-like bands near E_F are displayed[48]. Note that two sets of bands arise from the unit cell doubling along the c axis to represent the AFM order of Eu moments, which is adopted to the forced FM state in common[38]. In addition to a small change upon the spin flop of the Eu moments

[Figs. 4(a) and (b)], the splitting of red-colored (spin up) and blue-colored (spin down) bands progressively evolves, as the net magnetization (i.e., the canting of the Eu moment) increases in the spin-flop AFM phase [Figs. 4(b)−(d)]. Since the present calculation does not take $E_{\rm Z}$ into consideration, this large spin splitting originates from the exchange coupling of the Dirac fermion with the local Eu moments ($E_{\rm ex}$), which can be expressed as $E_{\rm ex} = J\langle S\rangle = J\chi H/g_J$, where J is the exchange integral, $\langle S\rangle$ is the component of Eu^{2+} spin along the field, $g_J(=2)$ is the Landé g factor for Eu^{2+}, and χ is the magnetic susceptibility. In the AFM phase, since the field is parallel to the easy axis of Eu spins, χ is a small parallel susceptibility and hence $E_{\rm ex}$ is negligible. On the other hand, in the spin-flop AFM phase, where the Eu spin axis changes to be transverse to the field, χ corresponds to a much larger transverse susceptibility[49]. In the latter phase, the Landau level splitting is caused by $E_{\rm ex}$ as well as $E_{\rm Z}$, which renormalizes the g^* value. From the energy splitting shown in Fig. 4(d), we obtain $E_{\rm ex} = 50-80$ meV[50] for $\langle S\rangle = 7/2$ (i.e., $J = 14-23$ meV), which is comparable to (or even larger than) $E_{\rm Z} \sim 13$ meV at $H = H_{\rm c} \sim 22$ T for $g^* \sim 10$. Thus, the exchange coupling should appreciably contribute to the observed apparent change in g^* upon the AFM phase. The reduction of g^* in the spin-flop AFM phase implies that the sign of J is opposite to that of pristine g^*, although a more quantitative estimation of these parameters is a future subject.

In conclusion, we observed spin-split Landau levels of quasi-two-dimensional Dirac fermions in a bulk antiferromagnet $EuMnBi_2$, which markedly depend on the field-tunable magnetic order of Eu moments. In addition to Zeeman splitting relevant to the large g factor, the Dirac-like band exhibits substantial exchange splitting due to the coupling with the local Eu moments. Such an interplay of the spin-orbit and exchange interactions in the present compound yields novel correlated Dirac fermion states in a solid, offering a promising approach to emerging topological spintronics.

The authors thank T. Osada, A. Tsukazaki and Y. Fuseya for helpful discussions. This work was partly supported by PRESTO, JST (Nos. JPMJPR16R2 and JPMJPR1412), Grant-in-Aid for Young Scientists A (No. 16H06015), Grant-in-Aid for Scientific Research A (No. 17H01195), and the Asahi Glass Foundation.

* Corresponding author: sakai@phys.sci.osaka-u.ac.jp

[1] O. Vafek, A. Vishwanath, Annu. Rev. Condens. Matter Phys. **5**, 83 (2014).

[2] K. S. Novoselov, A. K. Geim, S. V. Morozov, D. Jiang, M. I. Katsnelson, I. V. Grigorieva, S. V. Dubonos, A. A. Firsov, Nature **438**, 197 (2005).

[3] Y. Zhang, Y. W. Tan, H. L. Stormer, P. Kim, Nature **438**, 201 (2005).

[4] N. P. Armitage, E. J. Mele, and A. Vishwanath, Rev. Mod. Phys. **90**, 015001 (2018).

[5] L. Šmejkal, T. Jungwirth, and J. Sinova, Phys. Status Solidi RRL **11**, 1700044 (2017).

[6] L. Šmejkal, Y. Mokrousov, B. Yan, and A. H. MacDonald, Nat. Phys. **14**, 242 (2018).

[7] S. Nakatsuji, N. Kiyohara, and T. Higo, Nature **527**, 212 (2015).

[8] A. K. Nayak, J. E Fischer, Y. Sun, B. Yan, J. Karel, A. C. Komarek, C. Shekhar, N. Kumar, W. Schnelle, J. Kubler, C. Felser, and S. S. P. Parkin, Sci. Adv. **2**, e1501870 (2016).

[9] T. Suzuki, R. Chisnell, A. Devarakonda, Y.-T. Liu, W. Feng, D. Xiao, J. W. Lynn, and J. G. Checkelsky, Nat. Phys. **12**, 1119 (2016).

[10] M. Hirschberger, S. Kushwaha, Z. Wang, Q. Gibson, S. Liang, C. A. Belvin, B. A. Bernevig, R. J. Cava and N. P. Ong, Nat. Mater. **15**, 1161 (2016).

[11] X. Wan, A. M. Turner, A. Vishwanath, and S. Y. Savrasov, Phys. Rev. B **83**, 205101 (2011).

[12] W. W.-Krempa, G. Chen, Y. B. Kim, and L. Balents: Annu. Rev. Condens. Matter Phys. **5** (2014) 57.

[13] K. Kuroda, T. Tomita, M.-T. Suzuki, C. Bareille, A. A. Nugroho, P. Goswami, M. Ochi, M. Ikhlas, M. Nakayama, S. Akebi, R. Noguchi, R. Ishii, N. Inami, K. Ono, H. Kumigashira, A. Varykhalov, T. Muro, T. Koretsune, R. Arita, S. Shin, T. Kondo and S. Nakatsuji, Nat. Mater. **16**, 1090 (2017).

[14] J. Park, G. Lee, F. Wolff-Fabris, Y. Y. Koh, M. J. Eom, Y. K. Kim, M. A. Farhan, Y. J. Jo, C. Kim, J. H. Shim, and J. S. Kim, Phys. Rev. Lett. **107**, 126402 (2011).

[15] J. K. Wang, L. L. Zhao, Q. Yin, G. Kotliar, M. S. Kim, M. C. Aronson, and E. Morosan, Phys. Rev. B **84**, 064428 (2011).

[16] K. Wang, D. Graf, H. Lei, S. W. Tozer, and C. Petrovic, Phys. Rev. B **84**, 220401(R) (2011).

[17] L.-L. Jia, Z.-H. Liu, Y.-P. Cai, T. Qian, X.-P. Wang, H. Miao, P. Richard, Y.-G. Zhao, Y. Li, D.-M. Wang, J.-B. He, M. Shi, G.-F. Chen, H. Ding, and S.-C. Wang, Phys. Rev. B **90**, 035133 (2014).

[18] L. Li, K. Wang, D. Graf, L. Wang, A. Wang, and C. Petrovic, Phys. Rev. B **93**, 115141 (2016).

[19] Y. Y. Wang, Q. H. Yu and T. L. Xia, Chinese Phys. B **25**, 107503 (2016).

[20] A. F. May, M. A. McGuire, and B. C. Sales, Phys. Rev. B **90**, 075109 (2014).

[21] H. Masuda, H. Sakai, M. Tokunaga, Y. Yamasaki, A. Miyake, J. Shiogai, S. Nakamura, S. Awaji, A. Tsukazaki, H. Nakao, Y. Murakami, T. Arima, Y. Tokura, and S. Ishiwata, Science Advances **2**, e1501117 (2016).

[22] A. Wang, I. Zaliznyak, W. Ren, L. Wu, D. Graf, V. O. Garlea, J. B. Warren, E. Bozin, Yimei Zhu, and C. Petrovic, Phys. Rev. B **94**, 165161 (2016).

[23] S. Borisenko, D. Evtushinsky, Q. Gibson, A. Yaresko, T. Kim, M. N. Ali, B. Buechner, M. Hoesch, and R. J. Cava, arXiv: 1507.04847 (2015)

[24] J. Y. Liu, J. Hu, Q. Zhang, D. Graf, H. B. Cao, S. M. A. Radmanesh, D. J. Adams, Y. L. Zhu, G. F. Cheng, X. Liu, W. A. Phelan, J. Wei, M. Jaime, F. Balakirev, D. A. Tennant, J. F. DiTusa, I. Chiorescu, L. Spinu, and Z. Q. Mao, Nat. Mater. **16**, 905 (2017).

[25] J. Liu, J. Hu, H. Cao, Y. Zhu, A. Chuang, D. Graf, D. J. Adams, S. M. A. Radmanesh, L. Spinu, I. Chiorescu, and Z. Mao, Sci. Rep. **6**, 30525 (2015).

[26] S. Huang, J. Kim, W. A. Shelton, E. W. Plummer, and R. Jin, Proc. Natl. Acad. Sci. USA, **114**, 6256 (2017).

[27] G. Lee, M. A. Farhan, J. S. Kim, and J. H. Shim, Phys. Rev. B **87**, 245104 (2013).

[28] M. A.Farhan, G. Lee, and J. H. Shim, J. Phys.: Condens. Matter **26**, 042201 (2014).

[29] T. Ando, A. B. Fowler, and F. Stern, Rev. Mod. Phys. **54**, 437 (1982).

[30] F. J. Teran, M. Potemski, D. K. Maude, T. Andrearczyk, J. Jaroszynski, and G. Karczewski, Phys. Rev. Lett. **88**, 186803 (2002).

[31] Y. Zhang, Z. Jiang, J. P. Small, M. S. Purewal, Y.-W. Tan, M. Fazlollahi, J. D. Chudow, J. A. Jaszczak, H. L. Stormer, and P. Kim, Phys. Rev. Lett. **96**, 136806 (2006).

[32] A. F. Young, C. R. Dean, L. Wang, H. Ren, P. Cadden-Zimansky, K. Watanabe, T. Taniguchi, J. Hone, K. L. Shepard and P. Kim, Nat. Phys. **8**, 550 (2012).

[33] S. Jeon, B. B. Zhou, A. Gyenis, B. E. Feldman, I. Kimchi, A. C. Potter, Q. D. Gibson, R. J. Cava, A. Vishwanath and A. Yazdani, Nat. Mater. **13**, 851 (2014).

[34] Z. J. Xiang, D. Zhao, Z. Jin, C. Shang, L. K. Ma, G. J. Ye, B. Lei, T. Wu, Z. C. Xia, and X. H. Chen, Phys. Rev. Lett. **115**, 226401 (2015).

[35] Y. Liu, X. Yuan, C. Zhang, Z. Jin, A. Narayan, C. Luo, Z. Chen, L. Yang, J. Zou, X. Wu, S. Sanvito, Z. Xia, L. Li, Z. Wang and F. Xiu, Nat. Commun. **7**, 12516 (2016).

[36] Y. F. Guo, A. J. Princep, X. Zhang, P. Manuel, D. Khalyavin, I. I. Mazin, Y. G. Shi, and A.

T. Boothroyd, Phys. Rev. B **90**, 075120 (2014).

[37] Contribution of off-diagonal resistivity tensor (e.g., ρ_{zx}) is negligibly small in the investigated range of θ. See supplementary Fig. S2.

[38] See Supplemental Material [url] for details of the experimental and computational methods, analyses on the θ-dependent SdH oscillation, and estimation of the experimental Fermi energy, which includes Refs. [51–64].

[39] D. P. Druist, P. J. Turley, K. D. Maranowski, E. G. Gwinn, and A. C. Gossard, Phys. Rev. Lett. **80**, 365 (1998).

[40] M. Kuraguchi and T. Osada, Physica E **6**, 594 (2000).

[41] M. Kawamura, A. Endo, S. Katsumoto, Y. Iye, C. Terakura, and S. Uji, Physica B **298**, 48 (2001).

[42] I. A. Luk'yanchuk, Y. Kopelevich, Phys. Rev. Lett. **97**, 256801 (2006).

[43] G. P. Mikitik, Y. V. Sharlai, Phys. Rev. Lett. **82**, 2147 (1999).

[44] F. F. Fang and P. J. Stiles, Physical Review **174**, 823 (1968).

[45] K.Vakili, Y. P. Shkolnikov, E. Tutuc, E. P. De Poortere, and M. Shayegan, Phys. Rev. Lett. **92**, 226401 (2004).

[46] A. Tsukazaki, A. Ohtomo, M. Kawasaki, S. Akasaka, H. Yuji, K. Tamura, K. Nakahara, T. Tanabe, A. Kamisawa, T. Gokmen, J. Shabani, and M. Shayegan, Phys. Rev. B **78**, 233308 (2008).

[47] In general, $\theta = \theta_{\rm inv}$ corresponds to not only $E_{\rm Z}/E_{\rm c} = 0.5$ but also $E_{\rm Z}/E_{\rm c} = 1.5, 2.5, \ldots$. However, for the latter case, another minimum in amplitude should appear below $\theta \sim 65°$, which is not clearly discernible in the present measurements. For details, see supplementary Fig. S5.

[48] In Fig. 4, the energy origin corresponds to the Fermi energy for the undoped case, which is slightly lower than the energy of the valence-band top. This is because the calculated band structure is semimetallic for every panel presumably due to the well-known underestimation of the band gap in the GGA calculation. The calculated conduction-band bottom lies near the X point in analogy with $SrMnBi_2$[14].

[49] From the magnetization data[21], we have estimated $\chi_{||}$ and $\chi_{\perp}$ to be 5.4×10^{-3} and 1.4×10^{-1} emu/mol at 2 K, respectively.

[50] The magnitude of $E_{\rm ex}$ remains a few tens of meV irrespective of the magnitude of $+U$ correction. See supplementary Fig. S11.

[51] C. Bergemann, A. P. Mackenzie, S. R. Julian, D. Forsythe, and E. Ohmichi, Advances in Physics **52**, 639 (2003).

[52] J. Xiong, Y. Luo, Y. H. Khoo, S. Jia, R. J. Cava, and N. P. Ong, Phys. Rev. B **86**, 045314 (2012).

[53] J. P. Perdew, K. Burke, and M. Ernzerhof, Phys. Rev. Lett. **77**, 3865 (1996).

[54] G. Kresse and D. Joubert, Phys. Rev. B **59**, 1758 (1999).

[55] G. Kresse and J. Hafner, Phys. Rev. B **47**, 558(R) (1993).

[56] G. Kresse and J. Hafner, Phys. Rev. B **49**, 14251 (1994).

[57] G. Kresse and J. Furthmüller, Computational Materials Science **6**, 15 (1996).

[58] G. Kresse and J. Furthmüller, Phys. Rev. B **54**, 11169 (1996).

[59] A. I. Liechtenstein, V. I. Anisimov, and J. Zaanen, Phys. Rev. B **52**, R5467(R) (1995).

[60] S. L. Dudarev, G. A. Botton, S. Y. Savrasov, C. J. Humphreys, and A. P. Sutton, Phys. Rev. B **57**, 1505 (1998).

[61] N. Marzari and D. Vanderbilt, Phys. Rev. B **56**, 12847 (1997).

[62] I. Souza, N. Marzari, and D. Vanderbilt, Phys. Rev. B **65**, 035109 (2001).

[63] J. Kuneš, R. Arita, P. Wissgott, A. Toschi, H. Ikeda, and K. Held, Comp. Phys. Commun. **181**, 1888 (2010).

[64] A. A. Mostofi, J. R. Yates, Y.-S. Lee, I. Souza, D. Vanderbilt, and N. Marzari, Comput. Phys. Commun. **178**, 685 (2008).